Modeling, Control, and Operation of an M-DAB DC-DC Converter for Interconnection of HVDC Grids

Yazdi, Seyed Saeid Heidari; Rouzbehi, Kumars; Carrizosa, Miguel Jimenez; Heidary, Amir; Bagheri, Mehdi

DOI
10.1109/JSYST.2023.3235249

Publication date
2023

Document Version
Final published version

Published in
IEEE Systems Journal

Modeling, Control, and Operation of an M-DAB DC–DC Converter for Interconnection of HVDC Grids

Seyed Saeid Heidari Yazdi, Kumars Rouzbehi, *Senior Member, IEEE*, Miguel Jiménez Carrizosa, Amir Heidary, *Graduate Student Member, IEEE*, and Mehdi Bagheri, *Senior Member, IEEE*

***Abstract*—Future high-voltage direct-current (HVDC) networks based on voltage source converters (VSCs) will have different structures (asymmetric monopolar, bipolar, or symmetric monopolar), voltage levels, control, and protection schemes. Therefore, dc–dc converters are needed to interconnect those VSC-HVDC grids and several technical issues on their control and operational systems must be adequately addressed. A dc–dc converter based on a modular-dual active bridge (M-DAB) converter is suggested to reach a desirable interconnection of the HVDC grids and regulate power flow (PF) between them. A dynamic averaged model is proposed for the M-DAB converter and its stability is analyzed using the Lyapunov function. Moreover, a new local controller based on nonlinear control theory is proposed for the M-DAB. The new M-DAB local controller is integrated with the energy management system (EMS), by updating the PF equations, to create a complete control structure. Considering the CIGRE DCS3 HVDC test system and the studied M-DAB, static, dynamic simulation, and experimental studies are conducted and the dc–dc converter and the performance of the designed controllers and the EMS are examined and validated.**

***Index Terms*—DC–DC converter, HVDC grids interconnection, modular dual active bridge (M-DAB) converter, MT-HVDC grids, nonlinear control.**

I. Introduction

ADVANCEMENTS of the semiconductor industry have made the voltage source converters (VSC) based multiterminal HVDC (MT- HVDC) grids an ideal solution for integrating offshore renewable generators and onshore power systems, high power transmission in long distances, and interconnection of asynchronous ac networks [1], [2], [3]. Future VSC-HVDC grids might be asymmetric monopolar, bipolar, or symmetric monopolar and each type needs proper grounding structure. Those HVDC grids might also be from different rated voltage, converter technology, control, and protection philosophies [4]. Therefore, fully rated and highly reliable dc–dc converters should be employed to interconnect those HVDC grids. DC–DC converters can also act as a dc transformer, power flow controller (PFC), and dc circuit breaker [5], [6], [7], [8], [9].

For the discussed application, the step ratio of the dc–dc converter (n) is expected to be low ($1< n<1.5$) and it should transmit full power flowing between two HVDC grids in both directions. In this sense, it should be highly reliable, just like a transmission line. If the dc–dc converter is to be placed on an offshore substation, its footprint and weight should be minimized. This converter should prevent the propagation of dc faults to other healthy HVDC grids; thus, several protection zones will be formed. In this application, galvanic isolation is not crucial for component safety; however, it can reduce the complexities of the interconnection process (e.g., grounding coordination) and facilitate voltage stepping and blockage of dc fault. Several dc–dc converter topologies are recommended for the studied application; a comprehensive review of the available topologies is presented in [10], [11], [12]. On that basis, dc–dc converters can be divided into three groups.

The *first group* is based on dc–dc converters formed by a single branch, and the same (chopped) current can flow through the input and output terminals. They are typically restricted to two-port topologies and have a simple topology. Utilization of these converters in HVDC applications requires the construction of switch valves by combining single switches in series. Static and transient sharing of voltages between those series switches is challenging and cannot cope with the emerging high voltages [10].

The *second group* contains multiconversion stages converters, excluding modular multilevel converter (MMC) and its variations. They usually have two converter bridges and an internal ac circuit. High-power dc–dc converters include both nonisolated and isolated topologies. These dc–dc converters can interconnect a couple of dc grids with different nominal voltages. Three techniques are available for nonisolated converters to

Manuscript received 23 February 2022; revised 5 November 2022; accepted 19 December 2022. Date of publication 24 January 2023; date of current version 8 June 2023. This work was supported by the Collaborative Research Project (CRP) Grant, Nazarbayev University under Grant 021220CRP0322. *(Corresponding author: Mehdi Bagheri.)*

Seyed Saeid Heidari Yazdi and Mehdi Bagheri are with the School of Engineering and Digital Sciences (SEDS), Department of Electrical and Computer Engineering, Nazarbayev University, Astana 010000, Kazakhstan (e-mail: saedheidary@nu.edu.kz; mehdi.bagheri@nu.edu.kz).

Kumars Rouzbehi is with the Departamento de Ingeniería de Sistemas y Automática, Universidad de Sevilla, 41092 Sevilla, Spain (e-mail: krouzbehi@us.es).

Miguel Jiménez Carrizosa is with the Department of Electrical Engineering, Universidad Politécnica de Madrid, 28040 Madrid, Spain (e-mail: miguel.jimenezcarrizosa@upm.es).

Amir Heidary is with the IEPG group, Department of Electrical Sustainable Energy department, Delft University of Technology, 2628CD Delft, The Netherlands (e-mail: A.heidary@tudelft.nl).

Digital Object Identifier 10.1109/JSYST.2023.3235249

reach a high stepping-up/down voltage ratio: inductor-based, capacitor-based, and inductor-capacitor-based. How to realize isolation for the gate drivers, how best to organize the series connection of semiconductor devices, and how to obtain a desired electrical isolation between the generation and the dc link are challenging for nonisolated converters. Isolated converters utilize transformers to obtain the isolation as well as to manage the voltage step-up/down. Dual active bridge (DAB), dual half-bridge (DHB), and the series resonant converter are key isolated converters. Isolated transformers will provide galvanic isolation and optimize switch utilization. To maximize power transfer capability and efficiency, a suitable transformer should be designed and the system should be operating under a high switching frequency.

The *third group* consists of cascaded connections of individual dc–ac and ac–dc converters [13], [14], [15]. Various topologies (possibly MMC and its variants) can be utilized for ac–dc and dc–ac converters. However, the application of the classical MMC-based dc–dc converters operated by pulsewidth modulation typically requires a bulky ac transformer [16]. From the grid point of view, discussed cascaded combination can be regarded as a dc–dc converter.

It is necessary to identify a proper dc–dc converter to perform the role of the dc transformer and highly flexible PFC. Also, appropriate dynamic and static models should be proposed for the identified dc–dc converter. A control structure should also be proposed for the meshed HVDC grid. Said control structure should include local dc–dc converter controller and supervisory control center for the HVDC grids. Hence, the study approach and contributions of this article are as follows.

1) Several candidate topologies are presented and compared. Then, a suitable modular DAB (M-DAB) converter topology is suggested, evaluated, and utilized to study the static and dynamic aspects of the HVDC grids interconnection.
2) A dynamic averaged model is proposed for the M-DAB converter. Based on the proposed model, a methodology based on Lyapunov theory and a local nonlinear controller are proposed. They are to study and improve the asymptotic stability of M-DAB and their effective performance is studied by simulations and validated by experiments.
3) A comprehensive supervisory layer is proposed at the grid level by including the M-DAB converter in the power flow (PF) equations of the HVDC grids.
4) Performance of the M-DAB and grids' overall control framework is evaluated and analyzed. Set-point changes are applied to the power flowing from the HVDC line interconnecting two HVDC grids and also power generated by the wind farms. Both simulation and experimental studies are conducted.

II. Literature Review and Suggestion of M-DAB Power Converter and Related Controllers

A. Topology Selection and Design Criteria

It is desirable for dc transformers inserted into HVDC grids to i) offer high voltage scalability and galvanic isolations by

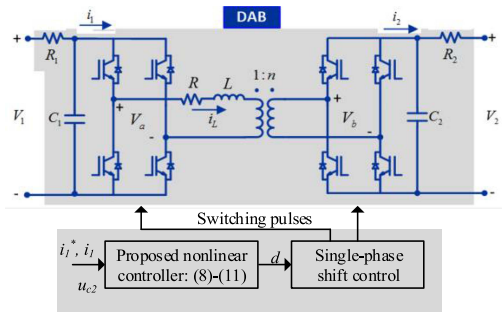

Fig. 1. Topology of DAB dc–dc converter.

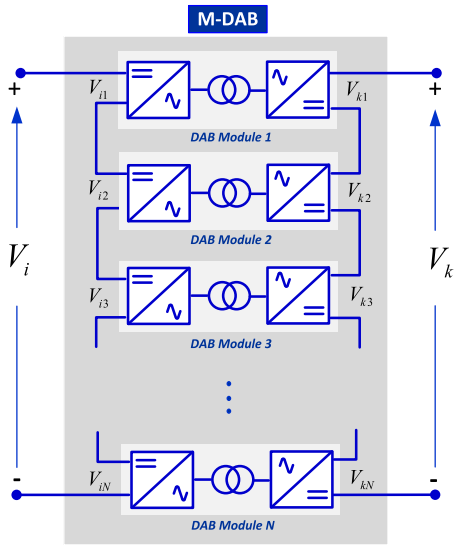

Fig. 2. Suggested modular DAB (M-DAB) power converter.

embodying an interlinking medium or high-frequency ac transformer. Therefore, reactive power circulation will be minimized; semiconductors of the higher voltage end will be better utilized; prevention of dc fault propagation will be easier; ii) apply low (*dv/dt*) voltage stress to windings of the interlink transformer, semiconductors, and other passive elements; iii) have minimized weight and size for the interlink transformer and overall footprint; iv) preclude propagation of the dc fault while preserving the safe operation of the converter, however, dc fault blocking capability is not required; v) have a wide range of modulation index to be able to support back-start of ac link and dc capacitors; and vi) be bidirectional and have high reliability [10], [11]. The focus is on high voltage (above 100 kV) and high power (above 500 MW) HVDC grids.

B. Suggested M-DAB Power Converter

The suggested M-DAB converter (see Fig. 2) consists of modules of bidirectional front-to-front DABs based on full bridges (see Fig. 1). Each full-bridge is connected to an input dc capacitor and winding of the interlink ac transformer and transmits a portion of the whole power. With a proper number of modules, M-DAB can be scaled to high-voltage, high-power applications and provide galvanic isolation. As low dc voltage

will exist at each module, low (*dv/dt*) voltage stresses will exist. Also, the frequency of semiconductors switching can be increased well above 1 kHz to reduce the weight and size of ac transformers. In industrial applications, the applied frequency is typically around 6 kHz for 10 MW and square wave modulation is adopted to reduce switching losses [17]. Weight reduction is less subject to the mechanical constraints of ac transformers and clearance spaces; because each module carries a fraction of the total power. DC fault inception at one converter side will induce inrush currents at the ac link that can be mitigated/controlled by blocking/controlling the healthy converter. Therefore, M-DAB satisfies all six desirable features, has high power density, and is a decent candidate for PFC and separation of the grid into several dc protection zones. Rich control philosophies exist for this reliable converter that can operate M-DAB in a wide modulation index range. However, complex insulation coordination for interlink ac transformers should be done.

Regarding the overall merits of the suggested M-DAB topology (see Fig. 2), it is identified to be one of the most competitive candidates for future HVDC grids. To conduct this study, a modular configuration (see Fig. 2) based on DAB technology (see Fig. 1) is utilized to reach high voltage and high power requirements. In Fig. 1, R_1 and R_2 model the series resistance of the two connected HVDC lines.

As shown in Fig. 1, a series inductance L is utilized as an energy transfer component. To transmit power in both directions, the control variable will be the time difference between the voltages applied in the inductance L, V_a, and V_b terminals. This control variable is called "phase shift ratio," d. The single-phase shift (SPS) control can be simply implemented to control the DAB devices. To obtain the average model of the DAB, the SPS control is used in this study due to its simplicity.

C. Comparative Study of the Suggested M-DAB Converter

Apart from M-DAB and as per discussions of [10], [11], candidates like 3-ph and two-level converter DAB [18], half-bridge-based MMC (HB-MMC), and some variant topologies of the MMC [19], [20], [21], [22] like controlled transition bridge (CTB)-DAB [23], [24], transition arm (TA)-MMC-DAB [25], alternative arm (AA)-MMC-DAB [26], and hybrid cascaded two-level converter-DAB [27] satisfy the desired features partly or completely. A detailed description of circuitries and the control/operation mechanism of those converters is reported in [10] and [11]. In this article, just a brief comparison will be provided.

Two-level mode operation is suggested for all concerned topologies, which have galvanic isolation, to reduce the converter footprint and switching losses. However, M-DAB has the lowest semiconductor elements (which facilitates size and weight reduction) and significantly lower conduction losses under the same voltage/power levels. HB-MMC (in multilevel operation), hybrid cascaded two-level converter-DAB, and AA-MMC-DAB have, respectively, maximum conduction losses; thus, their utilization is not favorable.

3-ph and two-level converter DAB's switch valves are constructed of a series of semiconductors and switches directly between $\pm 0.5 v_{\mathrm{dc}}$. Thus, it cannot operate in emerging high voltages due to the challenges of static and dynamic blockage voltage sharing and (*dv/dt*) voltage stress. The rest of the converters have acceptable voltage stresses.

In comparison with M-DAB, the possibility for weight/size reduction of magnetic elements by increasing fundamental ac frequency is lower for other converters. It is since they have more switches and their single ac transformer should be able to bear higher mechanical stresses and satisfy higher clearance distance; so, there will be volume constraints. For black start support capability, lower modulation indices will be required for two-level operated MMC, CTB-DAB, and TA-DAB, which will require higher cell capacitances and increased footprint in a reasonable range. This partly describes why M-DAB typically has a wider feasible modulation index range.

Regarding soft-switching abilities, most of the switches of the two-level operated MMC, CTB-DAB, and TA-DAB do not enjoy the zero-current turn-ON condition of the M-DAB's switches, where antiparallel diodes start conduction first. Regarding dc faults, all four M-DAB, two-level operated HB-MMC, CTB-DAB, and TA-DAB converters can alleviate fault propagation and none of them can block dc fault; thus, their freewheeling diodes will experience current stress for a short time. However, as two-level operated MMC and TA-DAB converters do not have input dc capacitors, they do not increase dc fault level.

D. Available Modulation Schemes and Control Methods for a Single DAB Converter

Studies on DAB converters mainly focus on switching/modulation strategies instead of outer current control schemes [28]. How to mitigate dc bias current (which happens in dynamic operation) is reviewed in [29] for different phase-shift modulations. Also, solutions to manage the circulating current and extend the zero voltage switching span are analyzed in [30]. The already available control methodologies for closed-loop (current) control methods are detailed in [31]. Those methods include linearization control, disturbance-observer-based control, and feedforward current control. Closed-loop impedance analyses were done to assess the dynamic performance in voltage/current reference tracking and load disturbance rejection. Indices like implementation complexity, dynamics performance, robustness against parameter variation, and implementation cost are assessed. It is concluded that the mentioned controllers have poor performance, considering the robustness against parameter variation.

The critical point is that most of the already available control methods focus on controlling the DAB converter's output dc voltage. In other words, they assume that one side of the DAB converter is connected to a stiff dc voltage, and they project to regulate the other side's dc voltage which will feed a constant impedance load. This is not the scenario when the suggested M-DAB converter interconnects two HVDC grids and acts as PFC/dc transformer. There exist very few research on the control design on this scenario, which is the focus of this research.

The suggested M-DAB converter aims to regulate the current flowing from the converter terminals. Little research exists on

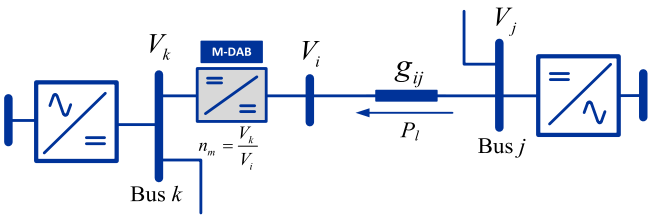

Fig. 3. M-DAB dc–dc converter placed between dc buses *j* and *k*.

the current control mode regulation of the DAB converters [32], [33]. SPS modulation are employed in [32], [33] and a linearized dynamic model of the converter is utilized. The linear proportional–integral (PI) controllers are used, and the tuning rules are derived based on the developed dynamic models. Linearized models of the DAB converters are obtained from the original nonlinear model in the vicinity of the prespecified operating point. In this sense, the linearized models and the tuned PI controller might not behave as designed in the operating points far from the operating point and stability margins might be affected.

III. Interconnection of VSC-HVDC Grids Using M-DAB Power Converter

A dc–dc converter is suggested in this research work, which is composed of an M-DAB power converter, to be installed between two VSC-HVDC grids. The proposed dynamic averaged models, nonlinear stability analysis, and nonlinear local controllers for single-module and *N*-module M-DAB converter will be given. Afterward, the PF problem of the interconnected HVDC grids will be formulated and the proposed method to include the suggested M-DAB converter in the static analysis will be described. Such integration helps to specify suitable control references for the grid's active elements and realize prespecified PF.

In Fig. 3, the M-DAB dc–dc converter and its associated line interconnect bus numbers *j* and *k,* which are assumed to have different dc voltage levels. Also, the dc–dc converter controls the PF of the dc line connected between buses *j* and *i*. Interconnection of buses *j* and *k* and PF control is realized by adjusting the M-DAB's transformation ratio, *nm*, from the grid's perspective

$$n_m = \left(\frac{V_k}{V_i}\right) \tag{1}$$

where V_i and V_k are the dc–dc converter's steady-state input and output voltages as illustrated in Fig. 3.

A. Single-Module DAB: Average Model

Since each combination of switching states provides a different electrical system, to model the power converter rigorously, it is necessary to solve a different differential equation for each combination. This way of proceeding is challenging; however, since these combinations are cyclic, an averaging method can contribute to obtaining a reliable model [34].

Consider a signal *f(t)*, which is not essentially cyclic. Its averaged value, $<f(t)>$, on a time interval of *T* can be obtained as

$$T\langle f(t)\rangle = \int_{t-\eta}^{t} f(\eta)\, d\eta. \tag{2}$$

The time derivative of an averaged signal equals its derivative´s sliding average

$$\frac{d}{dt}\langle f(t)\rangle = \left\langle \frac{d}{dt} f(t) \right\rangle. \tag{3}$$

Considering these premises and the averaging method, the state-space model of (4) could be obtained. In this model and as it is shown in Fig. 1, the average value of the input current i_1 is considered as the state variable, instead of the current through the inductance. The reasons are well explained in [35] and [36]; though, fundamentally, this is because inductance's average current would be zero in steady condition for a given control variable *d*. Consequently, the following model can be derived

$$\begin{bmatrix} \dot{\langle i_1\rangle} \\ \dot{\langle u_{C1}\rangle} \\ \dot{\langle u_{C2}\rangle} \end{bmatrix} = \begin{bmatrix} -\frac{R}{L} & 0 & \frac{T\cdot R}{L^2\cdot n} d\,(1-2\,|d|) \\ -\frac{1}{C_1} & -\frac{1}{R_1 C_1} & 0 \\ \frac{n}{C_2} & 0 & -\frac{1}{R_2 C_2} \end{bmatrix} \cdot \times \begin{bmatrix} \langle i_1\rangle \\ \langle u_{C1}\rangle \\ \langle u_{C2}\rangle \end{bmatrix} + \begin{bmatrix} 0 \\ \frac{V_1}{R_1 C_1} \\ \frac{V_2}{R_2 C_2} \end{bmatrix}. \tag{4}$$

Model (4) is nonlinear because the control variable is multiplied by the (state) variables. Since the intention is to regulate the PF between two interconnected HVDC grids, in this case, the main target would be to control the current i_1 using the control variable *d*. At steady-state, the voltage level of the capacitors C_1 and C_2 will reach the values estimated by the power model of the system.

B. Single-Module DAB: Nonlinear Stability Analysis

The M-DAB converter should be able to realize its control objective (e.g., regulation of power/current exchanged by two interconnected HVDC lines) even if severe transients (sudden change in the power exchange of VSCs or fault condition in ac or dc parts) occur. So, nonlinear controllers are preferred rather than linear controllers that only perform well under mild disturbances and when the system operates around the operating point that they are tuned for. Nonlinear system stability has been extensively analyzed [37], [38]. To apply Lyapunov theory, (4) should be expressed as

$$x' = C + Ax + B(d)x \tag{5}$$

where the following matrices present *A*, *B*, and *C* coefficients, respectively.

$$A = \begin{bmatrix} -\frac{R}{L} & 0 & 0 \\ -\frac{1}{C_1} & -\frac{1}{R_1 C_1} & 0 \\ \frac{n}{C_2} & 0 & -\frac{1}{R_2 C_2} \end{bmatrix}, C = \begin{bmatrix} 0 \\ \frac{V_1}{R_1 C_1} \\ \frac{V_2}{R_2 C_2} \end{bmatrix}$$

$$B=\begin{bmatrix}0 & 0 & \frac{T\cdot Rn}{L^2}d\left(1-2\left|d\right|\right)\\ 0 & 0 & 0\\ 0 & 0 & 0\end{bmatrix}, x=\begin{bmatrix}\langle i_1\rangle\\ \langle u_{C1}\rangle\\ \langle u_{C2}\rangle\end{bmatrix}. \quad (6)$$

There would be only a single control variable in equations; thus, d will be utilized to control $\langle i_1\rangle$ considering the PF requirements between two HVDC grids.

The tracking error is also defined as

$$\overset{\sim}{\langle i_1\rangle}=\langle i_1\rangle-\langle i_1\rangle^* \quad (7)$$

where $\langle i_1\rangle^*$ represents the reference for the variable. Considering symbols of Figs. 1 and 3, $\langle i_1\rangle^*$ should be calculated as $\langle i_1\rangle^*=P^*/\langle u_{C1}\rangle^*+(1/R_{\text{diff}})[(V_j-V_k)-(V_j^*-V_k^*)]$ where P^* is the power reference, R_{diff} is the differential droop slope, and superscript $*$ denotes the reference of a variable. The first term in the equation of $\langle i_1\rangle^*$ regulates the PF between HVDC grids; while, the second term emulates a virtual resistance on the connected line of Fig. 3 and adds to the overall stability during transients. The discussed virtual resistance will be zero in the specified operating points and all references in the equation of $\langle i_1\rangle^*$ will be specified later by the PF analysis.

To converge the current to the related set-point, energy is needed that can be expressed by a Lyapunov function as follows:

$$\nu=\frac{1}{2}(\langle i_1\rangle-\langle i_1\rangle^*)^2=\frac{1}{2}\overset{\sim}{\langle i_1\rangle}^2. \quad (8)$$

The time derivative of the defined Lyapunov function is as follows:

$$\dot{\nu}=\left(-\frac{R}{L}\overset{\sim}{\langle i_1\rangle}\langle i_1\rangle+\frac{TRn\overset{\sim}{\langle i_1\rangle}\langle u_{C2}\rangle}{L^2}(d-2d\left|d\right|)\right). \quad (9)$$

To obtain a negative derivative, we can select

$$-\frac{R}{L}\langle i_1\rangle+\frac{TRn\langle u_{C2}\rangle}{L^2}d\left(1-2\left|d\right|\right)=-\alpha.\overset{\sim}{\langle i_1\rangle} \quad (10)$$

with $\alpha>0$. Therefore

$$\dot{\nu}=-\alpha.\overset{\sim}{\langle i_1\rangle}^2<0,\forall\overset{\sim}{\langle i_1\rangle}\neq 0 \quad (11)$$

that shows the DAB converter is asymptotically stable. The proposed nonlinear controller can be implemented as shown in Fig. 1.

C. N-Module DAB: Generalized State-Space Modeling and Nonlinear Stability Analysis

The DAB state-space model can be generalized to M-DAB state-space model. Considering the state-space representation of (4) and Fig. 2, and taking into account that the converter is composed of N modules, the M-DAB's generalized state-space model could be written as

$$\dot{x}=\begin{bmatrix}A_1 & S_2 & \dots & S_N\\ S_2 & A_2 & \dots & S_N\\ \dots & \dots & \dots & \dots\\ S_N & S_N & \dots & A_n\end{bmatrix}.x+\begin{bmatrix}C_1\\ C_2\\ \dots\\ C_N\end{bmatrix} \quad (12)$$

where

$$A_j=\begin{bmatrix}-\frac{R}{L} & 0 & \frac{TRn_j}{L^2}d_j\left(1-2\left|d_j\right|\right)\\ -\frac{1}{C_{1j}} & -\frac{1}{R_1C_{1j}} & 0\\ \frac{n_j}{C_{1j}} & 0 & -\frac{1}{R_2C_{2j}}\end{bmatrix} \quad (13)$$

$$S_j=\begin{bmatrix}0 & 0 & 0\\ 0 & -\frac{1}{R_1C_{1j}} & 0\\ 0 & 0 & -\frac{1}{R_2C_{2j}}\end{bmatrix} \quad (14)$$

$$C_j=\begin{bmatrix}0\\ \frac{V_1}{R_1C_{1j}}\\ \frac{V_2}{R_2C_{2j}}\end{bmatrix}^T \quad (15)$$

$$x=\left[\langle i_{11}\rangle,\langle u_{C11}\rangle,\langle u_{C21}\rangle,\dots,\langle i_{1N}\rangle,\langle u_{C1N}\rangle,\langle u_{C2N}\rangle\right]^T. \quad (16)$$

The optimal performance of M-DAB is obtained when the duty cycle of all submodules are similar ($d_1=d_2=...=d_N=d$). The generalization of the proposed nonlinear controller is as follows:

Let ν_{MDAB} MDAB be the Lyapunov function associated with the system (12)

$$\nu_{\text{MDAB}}=\frac{1}{2}\left\langle\overset{\sim}{i_{11}}\right\rangle^2+\dots+\frac{1}{2}\left\langle\overset{\sim}{i_{1N}}\right\rangle^2. \quad (17)$$

To obtain a negative derivative for the generalized Lyapunov function, it is possible to select

$$-\frac{R}{L}\langle i_{1j}\rangle+\frac{TRn\langle u_{C2j}\rangle}{L^2}d\left(1-2\left|d\right|\right)=-\alpha_j\left\langle\overset{\sim}{i_{1j}}\right\rangle \quad (18)$$

with $\alpha_j>0$. Therefore

$$\dot{\nu_{\text{MDAB}}}=\sum_{j=1}^{N}-\alpha_j\left\langle\overset{\sim}{i_{1j}}\right\rangle^2<0 \quad (19)$$

and consequently, the M-DAB is asymptotically stable.

D. Formulation of DC PF Problem for Each VSC-HVDC Grid

The dc PF formulation for an N_B-bus HVDC grid initiates through applying the following equalities:

$$P_i=V_i.I_i=P_{Gi}-P_{Li};\ i=1:N_B. \quad (20)$$

In (20), P_i symbols the total injected power to bus i, P_{Gi} is the total generated power, and P_{Li} is the total absorbed power.

The conductance matrix will relate the net injected currents to the bus voltages

$$\underbrace{[\mathbf{I}]}_{N_B\times 1}=\underbrace{[\mathbf{G}]}_{N_B\times N_B}.\underbrace{[\mathbf{V}]}_{N_B\times 1}. \quad (21)$$

The $\mathbf{G}$ elements are specified in the following:

$$\mathcal{G}_{ii}=\sum_{j=1}^{N_B}(c_{ij}+c_{si}),\mathcal{G}_{ij}=-c_{ij};i,j\in\{1:N_B\}. \quad (22)$$

In (22), c_{ij} symbolizes the conductance that exists among bus i and bus j, and c_{si} symbolizes the conductance that exists between the ground and bus i.

Active power can be derived as a function of the system's voltages and conductance matrix elements as

$$P_i = V_i.\sum_{j=1}^{N_B}(\mathcal{G}_{ij}V_j) i = 1 : N_B. \tag{23}$$

To solve the PF problem, each dc bus should contain one variable. A dc bus can be a load bus (P-bus) with predetermined net injected power ($P_i = P_{i,\text{ref}}$) or a voltage bus (V-bus), with prespecified dc voltage ($V_i = V_{i,\text{ref}}$).

A slack bus in the dc PF problem guarantees the grid's power balance. Since the slack bus's voltage is predetermined, it should be removed from the PF equations. The Newton–Raphson (NR) PF algorithm is successfully applied to ac networks [39]; therefore, it is employed to address the PF equations.

Slack bus (V-bus) is considered to be the first bus of the MT-HVDC system. Also, the variables vector is defined as

$$\underbrace{[\mathbf{V}]}_{(N_B-1)\times 1} = \begin{bmatrix} V_2 & \dots & V_{N_B} \end{bmatrix}^T. \tag{24}$$

The vector of mismatch power, $\Delta\mathbf{P}$, is also given by

$$\underbrace{[\Delta\mathbf{P}]}_{(N_B-1)\times 1} = \begin{bmatrix} \Delta P_2 & \dots & \Delta P_{N_B} \end{bmatrix}^T \tag{25}$$

where its elements are calculated as follows:

$$\Delta P_i = -V_i\left(\sum_{j=1}^{N_B} G_j V_j\right) + P_i^*;\ i = 2 : N_B. \tag{26}$$

The update for the state variables, V_2, …, V_{NB} at iteration k is given by

$$\underbrace{[\mathbf{V}]^{k+1}}_{(N_B-1)\times 1} - \underbrace{[\mathbf{V}]^{k}}_{(N_B-1)\times 1} = \underbrace{[\Delta\mathbf{V}]^{k}}_{(N_B-1)\times 1} \tag{27}$$

$$\underbrace{[\Delta\mathbf{V}]^{k}}_{(N_B-1)\times 1} = \underbrace{\left([\mathbf{J}]^{k}\right)^{-1}}_{(N_B-1)\times(N_B-1)} \underbrace{[\Delta\mathbf{P}]^{k}}_{(N_B-1)\times 1} \tag{28}$$

that $\mathbf{J}$ symbols the Jacobian matrix

$$\underbrace{[\mathbf{J}]}_{(N_B-1)\times(N_B-1)} = [J_{ij}]_{i,j=2,\dots,N_B}, J_{ij} = -\partial P_i/\partial V_j \tag{29}$$

$$J_{ij} = \begin{cases} -2\mathcal{G}_{ii}.V_i - \sum\limits_{\substack{j=1\\ j\neq i}}^{N_B}(\mathcal{G}_{ij}.V_j), i = j \\ -\mathcal{G}_{ij}.V_i, i \neq j \end{cases} \tag{30}$$

E. Embedment of M-DAB DC–DC Converter Into the PF Equations

PF formulation of the HVDC grids should be modified to model their interconnection and control activities of the M-DAB dc–dc converter and form a combined energy management system (EMS). The M-DAB dc–dc converter adds a new control freedom degree to the combined PF problem and consequently can regulate the current/power exchange between two interconnected HVDC grids.

In this context, two N_{B1}-bus and N_{B2}-bus HVDC grids are assumed where the first bus of each HVDC grid is assumed to be its slack bus. Considering Fig. 3, it is assumed that the M-DAB dc–dc converter and its connected line interconnect the bus *k* of grid *A* and the bus *j* of grid *B*. Variables vector and mismatch vector of the first and second grid and the interconnected system are as (31)–(34), where superscripts *A* and *B* denote grids 1 and 2, respectively.

$$\underbrace{[\mathbf{V}^A]}_{(N_{B1}-1)\times 1} = \begin{bmatrix} V_2^A & \dots & V_{N_{B1}}^A \end{bmatrix}^T;$$

$$\underbrace{[\mathbf{V}^B]}_{(N_{B2}-1)\times 1} = \begin{bmatrix} V_2^B & \dots & V_{N_{B2}}^B \end{bmatrix}^T \tag{31}$$

$$\underbrace{[\mathbf{VarV}]}_{(N_{B1}+N_{B2}-1)\times 1} = \begin{bmatrix} \mathbf{V}^A & \mathbf{V}^B & n_m \end{bmatrix}^T \tag{32}$$

$$\underbrace{[\Delta\mathbf{P}^A]}_{(N_{B1}-1)\times 1} = \begin{bmatrix} \Delta P_2^A & \dots & \Delta P_{N_{B1}}^A \end{bmatrix}^T;$$

$$\underbrace{[\Delta\mathbf{P}^B]}_{(N_{B2}-1)\times 1} = \begin{bmatrix} \Delta P_2^B & \dots & \Delta P_{N_{B2}}^B \end{bmatrix}^T \tag{33}$$

$$\underbrace{[\Delta\mathbf{P}^{new}]}_{(N_{B1}+N_{B2}-1)\times 1} = \begin{bmatrix} \Delta\mathbf{P}^A & \Delta\mathbf{P}^B & \Delta P_{kj} \end{bmatrix}^T. \tag{34}$$

In (31)–(34), n_m and P_{kj} symbol M-DAB dc–dc converter's transformation ratio and PF between HVDC grids *A* and *B*. Also, $\mathbf{VarV}$ and $\Delta\mathbf{P}^{\text{new}}$ represent the combined system's variable vector and mismatch vector, respectively. Considering Fig. 3 and assuming lossless M-DAB dc–dc converter ($P_{kj} = P_{ij}$),P_{kj} can be expressed as follows:

$$P_{kj} = P_{ij} = V_k^A g_{ij}\left(\frac{V_k^A}{n_m} - V_j^B\right). \tag{35}$$

The line PF (P_{kj}) can be regulated at its reference value (P_{kj}^*) by the M-DAB dc–dc converter by manipulating its control variable (n_m). Therefore:

$$P_{kj}^* - P_{kj} = \Delta P_{kj}. \tag{36}$$

ΔP_{kj} and n_m are the new mismatch vector element and control variable, respectively.

Hence, after some calculations, the linearized PF equations for the interconnected system can be derived by extending those of each HVDC grid as follows:

$$\underbrace{\begin{bmatrix} \mathbf{J}^{A,\text{new}} & \partial\Delta\mathbf{P}^A/\partial\mathbf{V}^2 & \partial\Delta\mathbf{P}^A/\partial n_m \\ \partial\Delta\mathbf{P}^B/\partial\mathbf{V}^A & \mathbf{J}^{B,\text{new}} & \partial\Delta\mathbf{P}^B/\partial n_m \\ \partial\Delta P_{kj}/\partial\mathbf{V}^A & \partial\Delta P_{kj}/\partial\mathbf{V}^B & \partial\Delta P_{kj}/\partial n_m \end{bmatrix}^k}_{[\mathbf{J}^{\text{new}}]_{(N_{B1}+N_{B2}-1)\times(N_{B1}+N_{B2}-1)}}.$$

$$\underbrace{\begin{bmatrix}\Delta\mathbf{V}^A\\ \Delta\mathbf{V}^B\\ \Delta n_m\end{bmatrix}^k}_{[\Delta\mathbf{VarV}]} = \underbrace{\begin{bmatrix}\Delta\mathbf{P}^A\\ \Delta\mathbf{P}^B\\ \Delta P_{kj}\end{bmatrix}^k}_{\Delta\mathbf{P}^{\text{new}}}. \tag{37}$$

Elements present in the Jacobian matrix of the combined system of (37) can be readily calculated by (38)–(46) where *xy* subscript denote (*x*,*y*) element of the related matrix

$$\left(\underbrace{[\partial\Delta\mathbf{P}^A/\partial\mathbf{V}^B]}_{(N_{B1}-1)\times(N_{B2}-1)}\right)_{xy} = \begin{cases} V_k^A g_{ij} & x=k-1, y=j-1\\ 0 & else\end{cases} \tag{38}$$

$$\left(\underbrace{[\partial\Delta\mathbf{P}^A/\partial n_m]}_{(N_{B1}-1)\times 1}\right)_{x} = \begin{cases} g_{ij}\left(V_k^A/n_m\right)^2 & x=k-1\\ 0 & else\end{cases} \tag{39}$$

$$\left(\underbrace{[\mathbf{J}^{A,\text{new}}]}_{(N_{B1}-1)\times(N_{B1}-1)}\right)_{xy} = \begin{cases} \left(\mathbf{J}^A\right)_{xy} - 2g_{ij}\left(V_k^A/n_m\right)\\ \quad +g_{ij}V_j^B\\ ; x=k-1, y=k-1\\ \left(\mathbf{J}^A\right)_{xy} \quad else\end{cases} \tag{40}$$

$$\left(\underbrace{[\partial\Delta\mathbf{P}^B/\partial\mathbf{V}^A]}_{(N_{B2}-1)\times(N_{B1}-1)}\right)_{xy} = \begin{cases} 2g_{ij}V_k^A/n_m - g_{ij}V_j^B\\ ; x=j-1, y=k-1\\ 0 \quad else\end{cases} \tag{41}$$

$$\left(\underbrace{[\mathbf{J}^{B,\text{new}}]}_{(N_{B2}-1)\times(N_{B2}-1)}\right)_{xy} = \begin{cases} \left(\mathbf{J}^B\right)_{xy} - g_{ij}V_k^A x=j-1,\\ \qquad\qquad y=j-1\\ \left(\mathbf{J}^B\right)_{xy} \quad else\end{cases} \tag{42}$$

$$\left(\underbrace{[\partial\Delta\mathbf{P}^B/\partial n_m]}_{(N_{B2}-1)\times 1}\right)_{x} = \begin{cases} -g_{ij}\left(V_k^A/n_m\right)^2 & x=k-1\\ 0 & else\end{cases} \tag{43}$$

$$\left(\underbrace{[\partial\Delta P_{kj}/\partial\mathbf{V}^A]}_{1\times(N_{B1}-1)}\right)_{x} = \begin{cases} -2g_{ij}V_k^A/n_m + g_{ij}V_j^B\\ \qquad x=k-1\\ 0 \quad x\neq k-1\end{cases} \tag{44}$$

$$\left(\underbrace{[\partial\Delta P_{kj}/\partial\mathbf{V}^B]}_{1\times(N_{B2}-1)}\right)_{x} = \begin{cases} V_k^A g_{ij} & x=j-1\\ 0 & x\neq j-1\end{cases} \tag{45}$$

$$\partial\Delta P_{kj}/\partial n_m = g_{ij}\left(V_k^A/n_m\right)^2. \tag{46}$$

Equations (37)–(46) form the interconnected system's Jacobian matrix and its elements, which permit the introduction of the M-DAB dc–dc converter into the system's PF problem. Jacobian matrix elements in each iterate should be calculated using the variables calculated in the previous iterate. Hence, a value of **VarV** can be calculated by iterating (47) until the mismatch vector $\Delta\mathbf{P}$ falls below a prespecified threshold

$$\underbrace{[\mathbf{VarV}]}_{(N_{B1}+N_{B2}-1)\times 1}^{k+1} = \underbrace{\left([\mathbf{J}^{\text{new}}]^k\right)^{-1}}_{(N_{B1}+N_{B2}-1)\times(N_{B1}+N_{B2}-1)} \cdot \underbrace{[\Delta\mathbf{P}^{\text{new}}]}_{(N_{B1}+N_{B2}-1)\times 1} + \underbrace{[\mathbf{VarV}]}_{(N_{B1}+N_{B2}-1)\times 1}^{k}. \tag{47}$$

Once the values of **VarV are** calculated, the reference current for the M-DAB dc–dc converter (i_1^* in Fig. 1) and reference power and voltage for onshore VSC's (active power-dc voltage) droop controllers can be specified to realize the intended PF.

Note that previous studies did not consider static modeling of two HVDC grids interconnected and interconnected by a PFC. Instead, they have focused on a single HVDC grid compensated by a PFC.

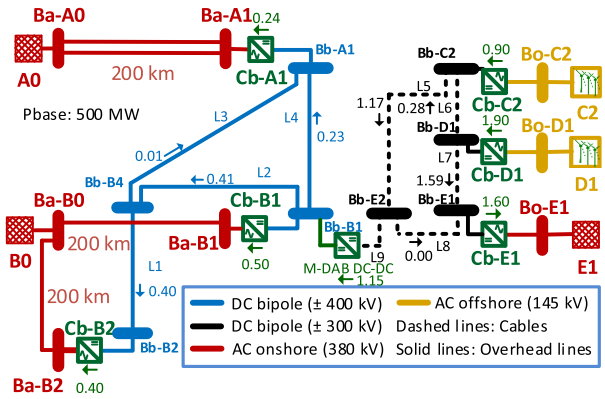

Fig. 4. CIGRE DCS3 grid and rounded results of PF in case of $n_m = 1$ (L_1: 300 km, L_2: 200 km, L_3: 500 km, L_4: 400 km, L_5: 200 km, L_6: 300 km, L_7: 200 km, L_8: 200 km, L_9: 200 km).

IV. Static and Dynamic Simulation Results

To evaluate the suggested M-DAB dc–dc converter and proposed (local and grid level) controllers, the modified CIGRE DCS3 MT-HVDC grid test system (see Fig. 4) was taken into account. In this modified grid, (2×800 MVA) Cb-E1 VSC is connected to bus Bb-E1 and buses Bb-C2 and Bb-E2 are interconnected by HVDC cable L5. Modeling and control of onshore grids/VSCs and offshore (aggregated) wind farms/VSCs are done according to the designs of [2]. In dynamic studies, onshore VSCs employ active power-dc voltage droop controllers as $P^* = P_0+(1/R)(V-V_0)$ for dc voltage regulation and active power sharing purposes. In that equation, P^*, P_0, V, V_0, and R denote reference and set-point power, measured and set-point dc voltage, and droop slope, respectively. The M-DAB dc–dc converter and its connected line (L9) are placed to interconnect the Bb-1 and Bb-E2 dc buses and control the interconnecting line's power. Per-unit parameters of the lines and other elements are specified in [40] and the M-DAB dc–dc converter parameters are presented in Table I.

Simulations studies are conducted using MATLAB m-file and Simulink platforms. Base power is assumed to be 500 MW and lines' power is calculated at their receiving side; thus, the sum

TABLE I
M-DAB DC-DC CONVERTER PARAMETERS

M-DAB DC-DC converter Parameters			
R_L	0.10 Ω	C_1	300 mF
		C_2	300 mF

TABLE II
PF ASSUMPTIONS

DC bus	Bus type	DC voltage	Net power (pu)
Bb-A1	Slack	1.00000	Unknown
Bb-B1	P	Unknown	-0.50000
Bb-B2	P	Unknown	-0.40000
Bb-B4	Intermediate	Unknown	0.00000
Bb-C2	P	Unknown	0.90000
Bb-D1	P	Unknown	1.90000
Bb-E1	Slack	1.00000	Unknown
Bb-E2	Intermediate	Unknown	0.00000

TABLE III
RESULT OF PF FOR HVDC GRID OF FIG. 4

DC bus/line	Base voltage	P^*_{ij} = 1.15 p.u., n_m=0.74421		P^*_{ij} = 1.3 p.u., n_m=0.74264	
		Voltage (pu)	**Power (pu)**	**Voltage (pu)**	**Power (pu)**
Bb-A1	800 kV	1.00000	-0.24832	1.00000	-0.39760
Bb-B1	800 kV	1.00164	-0.50000	1.00232	-0.50000
Bb-B2	800 kV	0.99801	-0.40000	0.99849	-0.40000
Bb-B4	800 kV	1.00015	0.00000	1.00063	0.00000
Bb-C2	600 kV	1.00621	0.90000	1.00577	0.90000
Bb-D1	600 kV	1.00843	1.90000	1.00826	1.90000
Bb-E1	600 kV	1.00000	1.60225	1.00000	1.45031
Bb-E2	600 kV	1.00003	0.00000	0.99941	0.0000
Bb-E2 to Bb-B1	-	-	1.15001	-	1.29999

of power in dc buses in Fig. 4 might not be zero due to lines' losses.

A. Modification in the Power Set-Point of the Controlled Line

In the first case study, the power flowing between bus Bb-E2 and bus Bb-B1 is changed through the control action of the M-DAB dc–dc converter. Basic PF assumptions are reported in Table II and the reference power for the M-DAB's line (L9 in Fig. 4) was initially 1.15 p.u. (i.e., the power is extracted from bus Bb-E2 and is injected into the bus Bb-B1). The related PF results are reported in Fig. 4 and Table III. The obtained values were then utilized to specify the reference control signals for onshore VSCs as well as the M-DAB dc–dc. Considering the M-DAB dc–dc, the PF solver provides the desired references current and bus voltage references and the local control system calculates the value of the desired control variable d to obtain the prespecified PF. From Table III, n_m is set to 0.74421 to realize both voltage matching and PF regulation objectives successfully.

At t = 4s, the controlled line's power is increased to 1.3 p.u. A new PF solution is derived to identify the reference control settings for onshore VSCs as well as the M-DAB dc–dc converter. The new PF results are also shown in Table III. From

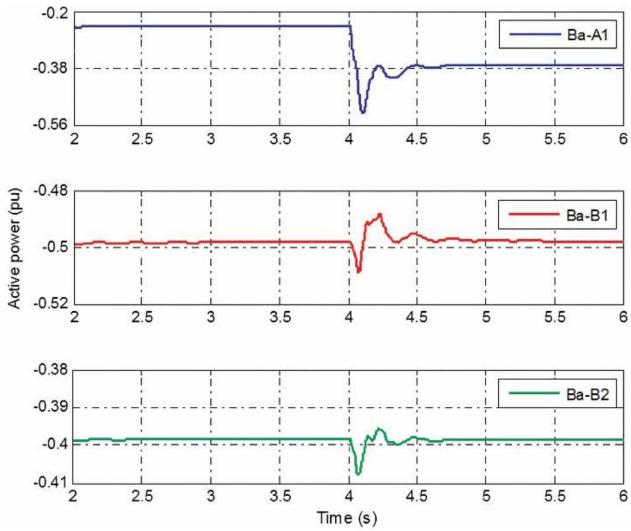

Fig. 5. Active powers of the onshore VSCs in case A.

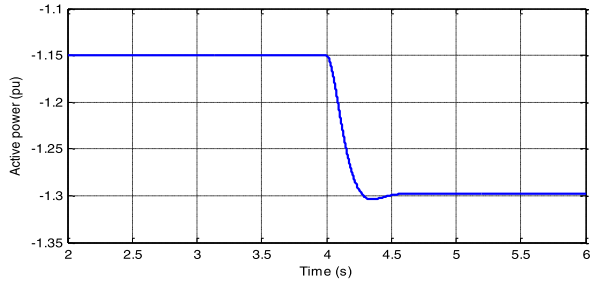

Fig. 6. Active power profile of the controlled HVDC line in case A.

Table III, n_m is reduced from 0.74421 down to 0.74264 to increase voltage differences across the M-DAB's line and hence inject more power from Bb-E2 into bus Bb-B1. Meanwhile, all PF assumptions for slack and P-buses are successfully enforced. The increase of power exchanged between two HVDC grids has also changed the power exchanged by slack buses to exert power balance and consider losses of the HVDC grids.

The powers flowing from the onshore ac converter stations and M-DAB's line power are shown in Figs. 5 and 6, respectively. Due to the M-DAB dc–dc converter's control action and proper reference control settings, the power through the controlled line is successfully changed to 1.3 p.u. after t = 4 s. Also, from the Fig. 7(a), the nonlinear controller successfully tracks the current reference by determining the proper phase shift for the SPS modulation scheme of the M-DAB converter, Fig. 7(b).

B. Grid Disturbances

The second simulation scenario focuses on grid disturbance [41]. To emulate the disturbance, the generated wind power of the Bb-D1 bus is decreased down to 1 p.u. from 1.9 p.u. at t = 5s. After the disturbance, the droop characteristics implemented at the primary level controls of onshore VSCs and also M-DAB dc–dc converter contribute to the dc voltage regulation and readjustment of the HVDC grid's PFs. This is obvious from

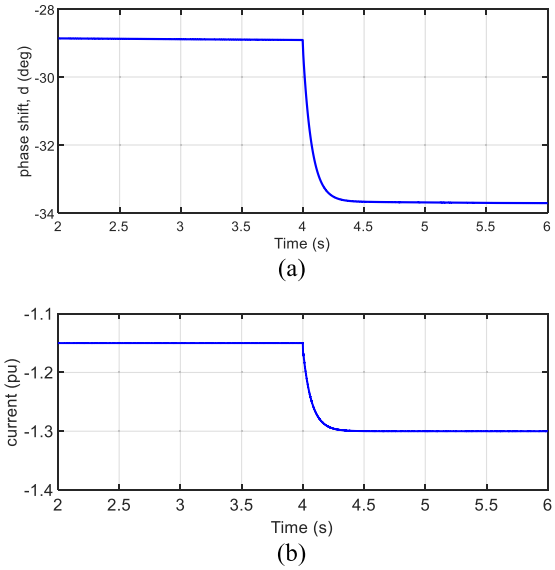

Fig. 7. Waveforms of the suggested M-DAB converter (a) Phase shift (in a single module) and (b) Flowing current toward the bus Bb-E2 of Fig. 4.

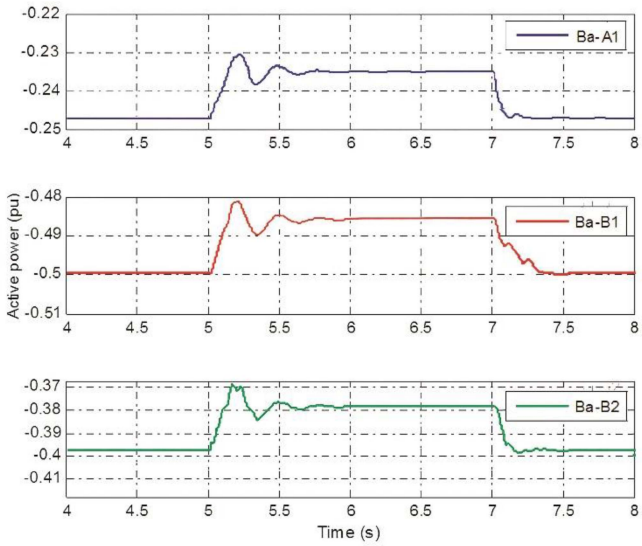

Fig. 8. Active powers of the onshore VSCs in case B.

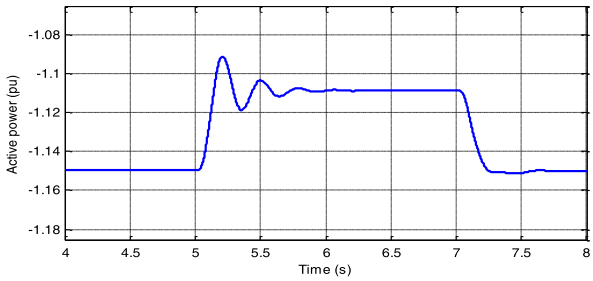

Fig. 9. Active power profile of the controlled HVDC line in case B.

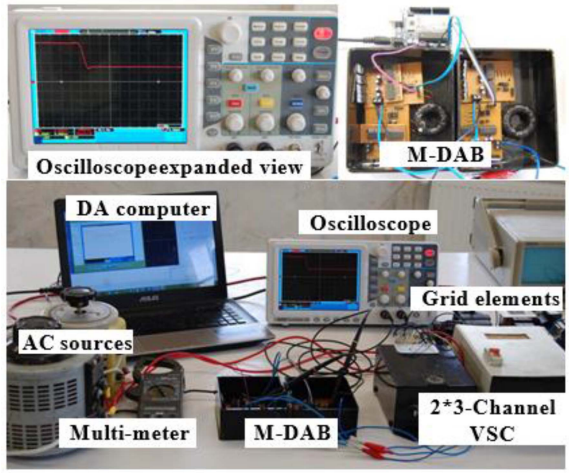

Fig. 10. Developed laboratory setup of M-DAB dc–dc converter.

TABLE IV
PARAMETERS AND DESCRIPTIONS OF THE PROTOTYPE

Symbol	Description	Nominal Values
M-DAB	Modular-DAB	0.5 kW, 100 V
VSC_1	Voltage Source Converter	0.5 kW, 100 V
VSC_2	Voltage Source Converter	0.5 kW, 100 V
Line	Wire and series impedance	0.1 Ω, 100 mH
V_{AC}	Voltage of the AC grids	98.9 V

the powers flowing from the onshore ac converter stations and the controlled HVDC line, which are shown in Figs. 8 and 9.

Afterward, at $t = 7$ s a new PF is executed; droop voltage references are calculated for onshore VSCs; and current reference and droop voltage references for the M-DAB dc–dc. It is to restore the compensated line's power to the prespecified value of 1.15 p.u. and the related dynamics are shown in Figs. 8 and 9. Observed dc voltages' profiles are within the permissible limits even during the transient periods; however, they are not shown due to the page limitations.

V. Experimental Validation

In this section, the performance of the M-DAB is validated based on a developed scaled-down prototype. The laboratory setup is depicted in Fig. 10 and its basic data is presented in Table IV. HGTP10N50C1 IGBT, toroid core (with cross-section of 2 cm^2 and length of 5 cm), C280 diodes, IR series gate drivers, and optoisolators is utilized to fabricate the DAB modules. The proposed nonlinear controller is implemented on the two-module M-DAB. The experimental setup comprises two-module M-DAB, two 3ph VSCs and a single dc line. AC sources were 380 V and 10 A single-phase autotransformers and controlled full bridge inverters were used to realize two three-channel VSCs. Two VSCs emulate two buses with different voltage values and the two-module M-DAB and the dc line interconnect those two buses and regulate the power exchange between them. OWON DS 5032E oscilloscope is utilized to record the signals.

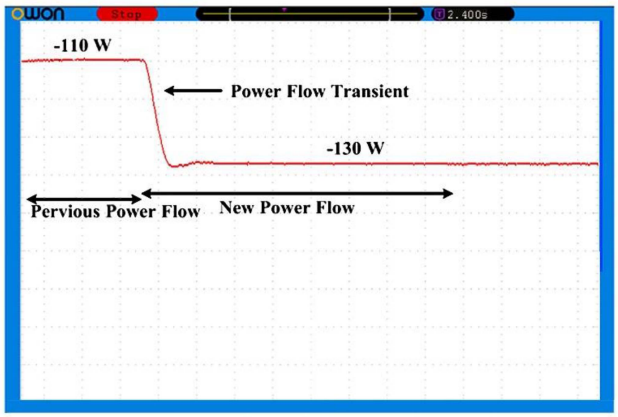

(a)

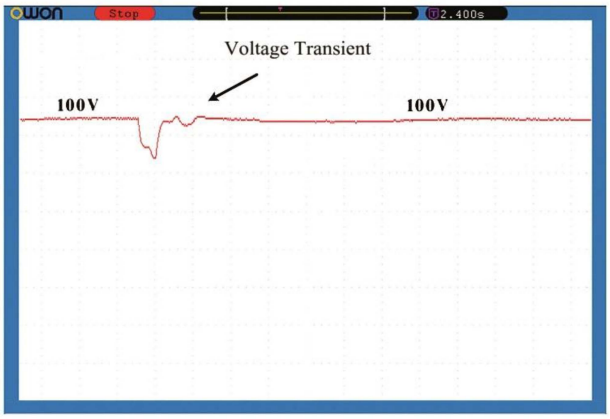

(b)

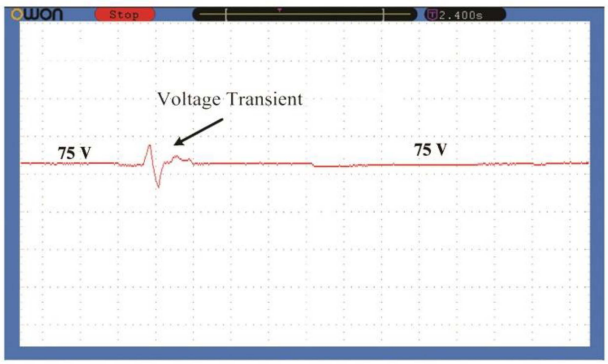

(c)

Fig. 11. Experimental results under step power increase of the M-DAB dc–dc converter: (a) PF profile, (b) dc bus voltage of the rectifying VSC, and (c) dc bus voltage of the inverting VSC.

A. Modification of PF

Over the first examination, the set-point of the PF in the tested line is changed from 110 to 130 W. The PF profile on the line is depicted in Fig. 11(a). Bus voltages are also shown in Fig. 11(b) and (c). From, Fig. 11(a), the M-DAB and its proposed controller can regulate the flowing power of the dc line and extract a prespecified amount of power from one dc bus and inject it into another dc bus. From Fig. 11(b) and (c), bus voltages are held constant, though they experience some transients, due to the action of VSCs in exerting fixed voltage values. Thus, the successful operation of the M-DAB dc–dc in interconnecting two buses with different voltages and regulation of PF exchange between them is proved.

(a)

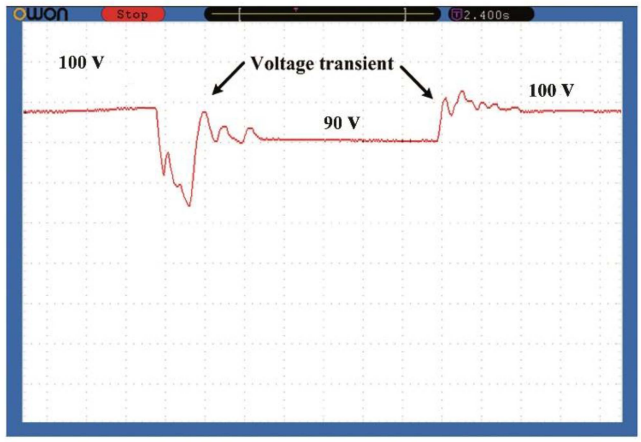

(b)

Fig. 12. Experimental results under grid disturbance and M-DAB operation: (a) PF profile and (b) dc bus voltage of the rectifying VSC.

B. PF Control in Grid Disturbance

For the second experiment, the condition of step power decrease of the rectifying VSC is emulated. For this emulation, the level of its dc voltage [see Fig. 12(b)] is stepped from 100 V down to 90 V while the dc voltage level of the inverting VSC is held constant. This is in line with the characteristics of the HVDC grids where the PF between lines depends on their differential voltages and resistances. So, for a dc bus (like a wind farm) to inject lower power into the HVDC grid, its dc voltage magnitude should be decreased.

Due to the disturbance condition and emulated virtual resistance, the power flowing from the M-DAB and its connected dc line [see Fig. 12(a)] is decreased from 82 to 72 W. After recalculation of the PF and updating the control references for the M-DAB dc–dc converter (voltage references for the emulated

virtual resistance and also the main term of current reference), the power flowing from the M-DAB and its connected dc line [see Fig. 12(a)] is decreased back to the 82 W. Therefore, successful operation of the M-DAB dc–dc converter under grid disturbances is shown.

VI. Future Work

It is expected to prevent the propagation of the dc fault between HVDC grids. M-DAB dc–dc converters can easily prevent dc fault propagation. This is done by monitoring the level of flowing currents and dc voltages, fast identification of the dc fault inception, and removing the gate signals of the power electronic switches for the involved DAB units. A comprehensive dc fault analysis of the suggested M-DAB converter, its impacts on dc fault protection (e.g., dc fault identification, isolation, coordinated operation of dc breakers and M-DAB, soft energization of the VSCs, M-DAB, and HVDC lines in post-dc fault) will be addressed in future research. Also, (large-signal) stability analysis of HVDC grids interconnected by a dc transformer using energy functions is an exciting research topic. In that research, nonlinear dynamics of ac/dc MMCs and associated complex controllers, dc overhead lines and cables, PFC and related controllers, and the interconnecting dc–dc converters should be considered.

VII. Conclusion

In this research work, a suitable M-DAB converter-based dc–dc converter was suggested for HVDC grids that can act as a flexible dc transformer and PF regulator. Suitable dynamic averaged models were proposed for the M-DAB converter. Based on the proposed dynamic models, the stability of the M-DAB converter was analyzed using Lyapunov theory and a local controller was proposed to ensure asymptotical stability for the converter. To integrate the proposed M-DAB dc–dc converter to the EMS of the MT-HVDC network, the required modifications in the dc PF algorithm were implemented.

Static analysis showed that the proposed PF integration method can successfully calculate variables and control references of both the HVDC grid and M-DAB dc–dc converter while interconnecting two distinct HVDC grids with different nominal voltages and regulating the exchanged PF between them. Dynamic simulations showed the successful performance of the M-DAB in HVDC grids interconnection and regulation of the PF between them and confirmed the satisfactory dynamics of the M-DAB dc–dc converter while adopting the proposed nonlinear controller. Changes in reference power of the regulated HVDC lines and the generated power of an offshore wind farm were considered case studies. Also, the results of experimental studies cross-verify the accuracy and effectiveness of the proposed nonlinear controller, EMS, and overall analysis.

References

[1] S. S. H. Yazdi, J. Milimonfared, S. H. Fathi, and K. Rouzbehi, "Optimal placement and control variable setting of power flow controllers in multi-terminal HVDC grids for enhancing static security," *Int. J. Elect. Power Energy Syst.*, vol. 102, pp. 272–286, 2018.

[2] S. S. H. Yazdi, J. Milimonfared, S. H. Fathi, and K. Rouzbehi, "A comprehensive VSG-based onshore FRT control strategy for OWFs with VSC-MT-HVDC transmission," *IEEE Access*, vol. 9, pp. 155788–155804, 2021.

[3] E. H. Kim, J. H. Kim, S. H. Kim, J. Choi, K. Y. Lee, and H. C. Kim, "Impact analysis of wind farms in the Jeju Island power system," *IEEE Syst. J.*, vol. 6, no. 1, pp. 134–139, Mar. 2012.

[4] A. Heidary, K. Rouzbehi, M. Hesami, M. Bigdeli, and C. Bordons, "Bridge-type fault current limiter and hybrid breaker for HVDC grids applications," *IET Gener., Transmiss. Distrib.*, vol. 14, pp. 3913–3919, 2020.

[5] K. Rouzbehi, J. I. Candela, A. Luna, G. B. Gharehpetian, and P. Rodriguez, "Flexible control of power flow in multiterminal DC grids using DC–DC converter," *IEEE J. Emerg. Sel. Topics Power Electron.*, vol. 4, no. 3, pp. 1135–1144, Sep. 2016, doi: 10.1109/JESTPE.2016.2574458.

[6] K. Rouzbehi, A. Miranian, A. Luna, and P. Rodriguez, "Towards fully controllable multi-terminal DC grids using flexible DC transmission systems," in *Proc. IEEE Energy Convers. Congr. Expo.*, 2014, pp. 5312–5316, doi: 10.1109/ECCE.2014.6954129.

[7] K. Rouzbehi, "Multi-terminal HVDC grids control and operation," M.S. thesis, Dept. d'Enginyeria Elèctrica, Universitat Politècnica de Catalunya-Barcelona Tech.-UPC, 2016.

[8] A. Heidary, H. Radmanesh, K. Rouzbehi, and J. Pou, "A DC-reactor-based solid-state fault current limiter for HVDC applications," *IEEE Trans. Power Del.*, vol. 34, pp. 720–728, Apr. 2019.

[9] M. Abbasipour, S. S. H. Yazdi, J. Milimonfared, and K. Rouzbehi, "Technical constrained power flow studies for IDC-PFC integrated into the MT-HVDC grids," *IEEE Trans. Power Del.*, vol. 36, no. 5, pp. 3033–3042, Oct. 2021.

[10] G. P. Adam, I. A. Gowaid, S. J. Finney, D. Holliday, and B. W. Williams, "Review of dc-dc converters for multi-terminal HVDC transmission networks," *IET Power Electron.*, vol. 9, pp. 281–296, 2016.

[11] J. D. Páez, D. Frey, J. Maneiro, S. Bacha, and P. Dworakowski, "Overview of DC–DC converters dedicated to HVDC grids," *IEEE Trans. Power Del.*, vol. 34, no. 1, pp. 119–128, Feb. 2019.

[12] O. Gomis-Bellmunt, J. Sau-Bassols, E. Prieto-Araujo, and M. Cheah-Mane, "Flexible converters for meshed HVDC grids: From flexible AC transmission systems (FACTS) to flexible DC grids," *IEEE Trans. Power Del.*, vol. 35, no. 1, pp. 2–15, Feb. 2020.

[13] T. Lüth et al., "Performance of a DC/AC/DC VSC system to interconnect HVDC systems," in *Proc. 10th IET Int. Conf. AC DC Power Transmiss.*, 2012, pp. 1–6.

[14] M. J. Carrizosa et al., "Stability of DC/DC three terminals converter using modular multilevel converters for HVDC systems," in *Proc. 17th Eur. Conf. Power Electron. Appl.*, 2015, pp. 1–10.

[15] J. Shi, W. Gou, H. Yuan, T. Zhao, and A. Q. Huang, "Research on voltage and power balance control for cascaded modular solid-state transformer," *IEEE Trans. Power Electron.*, vol. 26, no. 4, pp. 1154–1166, Apr. 2011.

[16] S. P. Engel, M. Stieneker, N. Soltau, S. Rabiee, H. Stagge, and R. W. D. Doncker, "Comparison of the modular multilevel DC converter and the dual-active bridge converter for power conversion in HVDC and MVDC grids," *IEEE Trans. Power Electron.*, vol. 30, no. 1, pp. 124–137, Jan. 2015.

[17] H. Fan and H. Li, "High frequency high efficiency bidirectional DC-DC converter module design for 10 kVA solid state transformer," in *Proc. 25th Annu. IEEE Appl. Power Electron. Conf. Expo.*, 2010, pp. 210–215.

[18] R. W. De Doncker, D. M. Divan, and M. H. Kheraluwala, "A three-phase soft-switched high-power-density DC/DC converter for high-power applications," *IEEE Trans. Ind. Appl.*, vol. 27, no. 1, pp. 63–73, Jan./Feb. 1991.

[19] H. Yang, M. Saeedifard, and A. Yazdani, "An enhanced closed-loop control strategy with capacitor voltage elevation for the DC–DC modular multilevel converter," *IEEE Trans. Ind. Electron.*, vol. 66, no. 3, pp. 2366–2375, Mar. 2019.

[20] S. Kaler and A. Yazdani, "Modeling and current-mode control of a DC–DC modular multilevel converter," *IEEE Trans. Ind. Electron.*, vol. 68, no. 11, pp. 10826–10834, Nov. 2021.

[21] R. Razani and Y. A. R. I. Mohamed, "Operation limits of the hybrid DC/DC modular multilevel converter for HVDC grids connections," *IEEE J. Emerg. Sel. Topics Power Electron.*, vol. 9, no. 4, pp. 4459–4469, Aug. 2021.

[22] S. Dey and T. Bhattacharya, "Operation of a modular DC–DC converter for hybrid interconnection of monopolar and bipolar HVDC links," *IEEE Trans. Ind. Appl.*, vol. 58, no. 4, pp. 4943–4954, Jul./Aug. 2022.

[23] U. K. Madawala and D. J. Thrimawithana, "Modular-based inductive power transfer system for high-power applications," *IET Power Electron.*, vol. 5, no. 7, pp. 1119–1126, 2012.
[24] C. Oates, K. Dyke, and D. Trainer, "The use of trapezoid waveforms within converters for HVDC," in *Proc. 16th Eur. Conf. Power Electron. Appl.*, 2014, pp. 1–10.
[25] I. A. Gowaid, G. P. Adam, B. W. Williams, A. M. Massoud, and S. Ahmed, "The transition arm multilevel converter — A concept for medium and high voltage DC-DC transformers," in *Proc. IEEE Int. Conf. Ind. Technol.*, 2015, pp. 3099–3104.
[26] T. Lüth, M. M. C. Merlin, T. C. Green, F. Hassan, and C. D. Barker, "High-frequency operation of a DC/AC/DC system for HVDC applications," *IEEE Trans. Power Electron.*, vol. 29, no. 8, pp. 4107–4115, Aug. 2014.
[27] Y. Zhang, G. P. Adam, T. C. Lim, S. J. Finney, and B. W. Williams, "Hybrid multilevel converter: Capacitor voltage balancing limits and its extension," *IEEE Trans. Ind. Inform.*, vol. 9, no. 4, pp. 2063–2073, Nov. 2013.
[28] N. Hou and Y. W. Li, "Overview and comparison of modulation and control strategies for a nonresonant single-phase dual-active-bridge DC–DC converter," *IEEE Trans. Power Electron.*, vol. 35, no. 3, pp. 3148–3172, Mar. 2020.
[29] Q. Bu, H. Wen, H. Shi, and Y. Zhu, "A comparative review of high-frequency transient DC bias current mitigation strategies in dual-active-bridge DC–DC converters under phase-shift modulations," *IEEE Trans. Ind. Appl.*, vol. 58, no. 2, pp. 2166–2182, Mar./Apr. 2022.
[30] S. Shao, H. Chen, X. Wu, J. Zhang, and K. Sheng, "Circulating current and ZVS-on of a dual active bridge DC-DC converter: A review," *IEEE Access*, vol. 7, pp. 50561–50572, 2019.
[31] S. Shao et al., "Modeling and advanced control of dual-active-bridge DC–DC converters: A review," *IEEE Trans. Power Electron.*, vol. 37, no. 2, pp. 1524–1547, Feb. 2022.
[32] M. Gierczynski, L. M. Grzesiak, and A. Kaszewski, "Cascaded voltage and current control for a dual active bridge converter with current filters," *Energies*, vol. 14, 2021, Art. no. 6214.
[33] S. Wei, Z. Zhao, K. Li, L. Yuan, and W. Wen, "Deadbeat current controller for bidirectional dual-active-bridge converter using an enhanced SPS modulation method," *IEEE Trans. Power Electron.*, vol. 36, no. 2, pp. 1274–1279, Feb. 2021.
[34] S. BachaIulian, M. Antoneta, and I. Bratcu, *Power Electronic Converters Modeling and Control With Case Studies*. Berlin, Germany: Springer–Verlag, 2014.
[35] M. J. Carrizosa, "Hierarchical control scheme for multi-terminal high voltage direct current power networks," Ph.D. dissertation, Université Paris Sud - Paris XI, Bures-sur-Yvette, France, 2015.
[36] M. J. Carrizosa, A. Benchaib, P. Alou, and G. Damm, "DC transformer for DC/DC connection in HVDC network," in *Proc. 15th Eur. Conf. Power Electron. Appl.*, 2013, pp. 1–10.
[37] H. Khalil, *Nonlinear Systems*, 3rd ed. Englewood Cliffs, NJ, USA: Prentice-Hall, 2002.
[38] *Bilinear Control Processes: With Applications to Engineering, Ecology, and Medicine*. Cambridge, MA, USA: Academic, 1973.
[39] N. M. Peterson and W. S. Meyer, "Automatic adjustment of transformer and phase-shifter taps in the newton power flow," *IEEE Trans. Power App. Syst.*, vol. PAS-90, no. 1, pp. 103–108, Jan. 1971.
[40] T. K. Vrana, Y. Yang, D. Jovcic, S. Dennetière, J. Jardini, and H. Saad, "The CIGRE B4 DC grid test system," *Electra*, vol. 270, no. 1, pp. 10–19, Oct. 2013.
[41] O. Abedinia, M. Bagheri, M. S. Naderi, and N. Ghadimi, "A new combinatory approach for wind power forecasting," *IEEE Syst. J.*, vol. 14, no. 3, pp. 4614–4625, Sep. 2020.